Correspondence to:
G. Foti,
g.foti@noc.ac.uk

Spaceborne GNSS reflectometry for ocean winds: First results from the UK TechDemoSat-1 mission

Giuseppe Foti[1], Christine Gommenginger[1], Philip Jales[2], Martin Unwin[2], Andrew Shaw[3], Colette Robertson[1], and Josep Roselló[4]

[1]National Oceanography Centre, Southampton, UK, [2]Surrey Satellite Technology Limited, Guildford, UK, [3]Skymat Limited, Southampton, UK, [4]ESTEC, European Space Agency, Noordwijk, Netherlands

Abstract First results are presented for ocean surface wind speed retrieval from reflected GPS signals measured by the low Earth orbiting UK TechDemoSat-1 satellite (TDS-1). Launched in July 2014, TDS-1 provides the first new spaceborne Global Navigation Satellite System-Reflectometry (GNSS-R) data since the pioneering UK-Disaster Monitoring Mission (UK-DMC) experiment in 2003. Examples of onboard-processed delay-Doppler maps reveal excellent data quality for winds up to 27.9 m/s. Collocated Advanced Scatterometer (ASCAT) winds are used to develop and evaluate a wind speed algorithm based on signal-to-noise ratio (SNR) and the bistatic radar equation. For SNRs greater than 3 dB, wind speed is retrieved without bias and a precision around 2.2 m/s between 3 and 18 m/s even without calibration. Exploiting lower SNR signals, however, requires good knowledge of the antenna beam, platform attitude, and instrument gain setting. This study demonstrates the capabilities of low-cost, low-mass, and low-power GNSS-R receivers ahead of their launch on the NASA Cyclone GNSS (CYGNSS) constellation in 2016.

1. Introduction

Global Navigation Satellite System-Reflectometry (GNSS-R) is an innovative Earth observation technique that exploits signals of opportunity from Global Navigation Satellite System (GNSS) constellations after reflection on the Earth surface. In brief, navigation signals from GNSS transmitters such as those of the Global Positioning System (GPS) are forward scattered off the Earth surface in the bistatic specular direction. Dedicated GNSS-R receivers on land, airborne, or spaceborne platforms detect and cross-correlate the reflected signals with direct signals from the same GNSS transmitter to provide geophysical information about the reflecting surface. An excellent comprehensive review of the GNSS-R technique was produced recently by *Zavorotny et al.* [2014].

GNSS-R can provide geophysical information about a number of surface properties, its applications to Earth observation, including remote sensing of ocean roughness, soil moisture, snow depth, and sea ice extent [see, for example, *Gleason*, 2006; *Cardellach et al.*, 2011]. The exploitation of GPS signals for ocean scatterometry was first proposed by *Hall and Cordey* [1988], and the first collection and tracking of reflected GPS navigation signals from an aircraft took place in July 1991 [*Auber et al.*, 1994]. In 1993, *Martin-Neira* [1993] proposed, for the first time, to use GPS reflectometry for mesoscale altimetry. Applications to ocean remote sensing have received by far the most attention to date, with many more studies focused on the retrieval of sea surface height [e.g., *Lowe et al.*, 2002; *Ruffini et al.*, 2004; *Nogues-Correig et al.*, 2010; *Carreno-Luengo et al.*, 2013] and ocean surface wind speed or mean square slope [e.g., *Garrison et al.*, 1998; *Rius et al.*, 2002; *Komjathy et al.*, 2004; *Katzberg et al.*, 2006; *Clarizia et al.*, 2009]. GNSS-R ocean roughness data can also contribute to better ocean salinity retrieval by providing better correction for sea state effects [e.g., *Valencia et al.*, 2011]. This paper focuses on the wind speed retrieval capability of GNSS-R.

The interest in GNSS-R for ocean wind monitoring stems primarily from the low-cost, low-mass, and low-power characteristics of GNSS-R receivers, which could lead to affordable multisatellite constellations able to deliver dramatically improved space/time sampling to complement existing ocean surface wind observations. With large and growing numbers of GNSS surface reflections available simultaneously at any point and time from GPS and other GNSS constellations (e.g., GLONASS, Galileo, Beidou, etc.), the technique also offers the possibility of wide-swath sensing given appropriate receiver and antenna specifications. Finally, GNSS-R uses

GNSS L-band microwave signals (~1.5 GHz, around 20 cm wavelength) which are less sensitive to atmospheric attenuation by precipitation than higher microwave frequencies and could therefore yield more robust wind estimates in heavy rain conditions.

While the literature reports many land-based and airborne GNSS-R experiments, there has been until now only limited spaceborne GNSS-R data. To gauge the potential of GNSS-R for improved global sampling, the technique needs to be convincingly demonstrated from low Earth orbiting (LEO) altitudes. Initial proof of concept from LEO was achieved in 2003/2004 with the pioneering GNSS-R experiment by Surrey Satellite Technology Ltd on the UK-Disaster Monitoring Mission (UK-DMC). About 50 separate data acquisitions were performed over the ocean [*Gleason*, 2006], although only a handful ever became available to the wider community for analysis [*Gleason and Gebre-Egziabher*, 2009; *Clarizia et al.*, 2009]. Ultimately, even the complete UK-DMC GNSS-R ocean data set is insufficient to provide a statistically robust assessment of the capabilities of GNSS-R from LEO altitude. The situation changed radically following the successful launch by Surrey Satellite Technology Ltd. on 8 July 2014 of the UK TechDemoSat-1 satellite and its GNSS-R payload.

This paper gives an overview of the GNSS-R experiment on TechDemoSat-1 and of the large GNSS-R data set acquired over the global ocean since 1 September 2014. Examples are shown of the onboard-processed delay-Doppler maps (DDMs) collected in different wind conditions, revealing excellent quality of the reflected signals for winds up to 27.9 m/s. The paper then presents an SNR-based inversion algorithm developed for the retrieval of ocean surface wind speed and preliminary validation results of TDS-1 wind speed against collocated wind measurements from the METOP ASCAT satellites. The final section highlights the specific technical constraints affecting GNSS-R wind retrieval on TDS-1 and indicates future work needed to fully demonstrate the wide-swath capabilities of the technique.
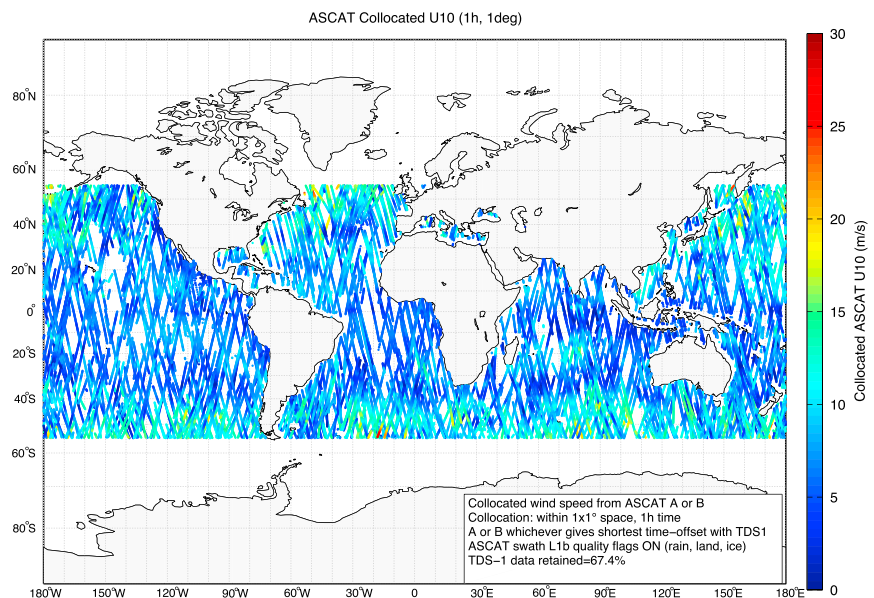
2. GNSS-R on TechDemoSat-1

The TechDemoSat-1 satellite was successfully launched on 8 July 2014 from the Baikonur launch site onboard a Soyuz launch vehicle. TDS-1 is a UK-funded technology demonstrator satellite which carries eight experimental payloads including the Space GNSS Receiver Remote Sensing Instrument (SGR-ReSI). The ReSI is a precursor of the GNSS-R receivers to be flown on the NASA Cyclone Global Navigation System Satellite (CYGNSS); [*Ruf et al.*, 2012] constellation of eight microsatellites due for launch in late 2016. The ReSI is a small (~300 × 160 × 30 mm), low-mass (~1.5 kg), low-power (~10 W) receiver based on commercial off-the-shelf components. Full details about TDS-1 and the ReSI can be found in *Jales and Unwin* [2015].

The TDS-1 satellite was placed into orbit at an altitude around 635 km with an inclination of 98.4°. The orbit is quasi Sun synchronous with a local time ascending node (LTAN) drift of 1.42 h/yr. The TDS-1 orbital elements are available from NORAD Celestrak with identifier "TDS 1" 40076. Satellite attitude knowledge comes from an onboard Kalman filter that takes inputs from magnetometers and Sun sensors. Attitude knowledge error is estimated to be around 1° in the noneclipsed part of the orbit and around 10° when the satellite is in eclipse.

The satellite is controlled and operated from the ground station with a strict 8 day duty cycle shared between the eight experimental payloads. The ReSI can be accessed and operated for only 2 days in every 8 day cycle. The baseline operation of the ReSI is for continuous acquisition of delay-Doppler maps (DDMs) generated onboard at 1 Hz with a coherent integration time of 1 ms. Although integration parameters of the onboard DDM processing are reprogrammable, this capability has not been exploited so far.

The ReSI collects GPS L-band L1 Coarse Acquisition signals using a highly directional downward pointing antenna with a peak gain of 13.3 dBi and a 3 dB half-beamwidth of 15°. The main lobe of the antenna is pointing 6° from the vertical behind the spacecraft. The ReSI is able to track, record, and process reflected signals simultaneously from four separate GPS transmitters (identified by their individual Pseudo Random Noise (PRN) codes). An onboard-ranking computation selects the four best specular reflections based on the closest proximity to the maximum gain of the receiver antenna.

The ReSI instrument can operate in two reprogrammable receiver gain modes: unmonitored automatic gain control (uAGC) or fixed gain mode (FGM). All ReSI data acquired up to 5 February 2015 were obtained in uAGC mode. While there are plans for acquisitions in FGM in the future, for the time being, in the absence of receiver gain data, analyses are limited to uAGC mode signals.

Figure 1. Geographical distribution of TDS-1 GNSS-R data acquired over the ocean between 1 September 2014 and 6 February 2015. Color indicates the wind speed measured by ASCAT (A or B, whichever is closest) within 1 h and 1° of latitude/longitude of the TDS-1 data. Standard ASCAT flags are applied. Data affected by sea ice are removed by limiting analyses to ocean data at latitudes below 55°.
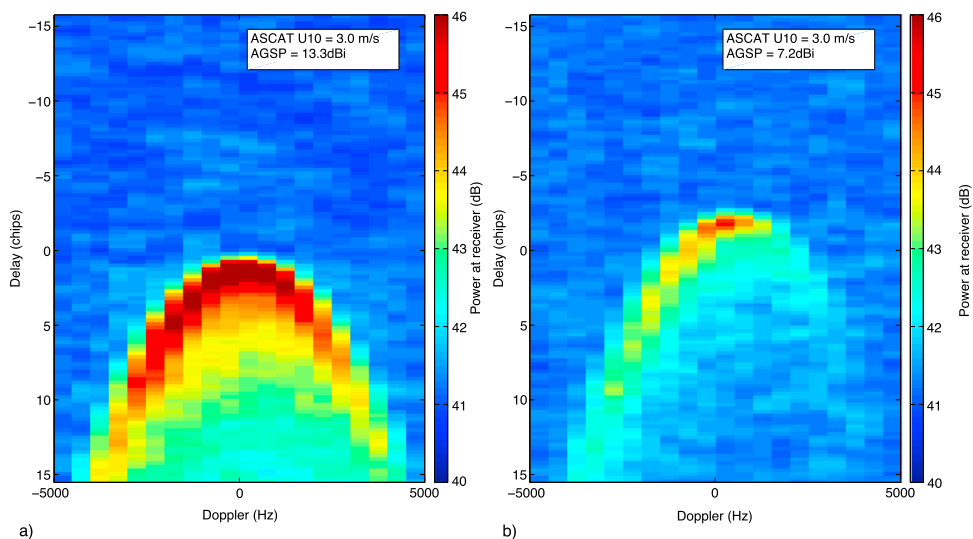
3. TDS-1 ReSI Data Collections

The first scientific data acquisition with TDS-1 ReSI took place on 1 September 2014. Since then, the ReSI has collected data at regular intervals, the volume of data collected in each duty cycle increasing steadily with time. As of 5 February 2015, the ReSI had acquired 3500 independent tracks across all GPS PRN, corresponding to over 1.5 million onboard-processed 1 Hz DDMs. The largest data set collected so far in 1 day represents approximately 20 h of data. Figure 1 shows the geographical distribution of the TDS-1 ReSI data acquired over the ocean between 1 September 2014 and 5 February 2015 across all PRN. Colors represent the collocated wind measurements obtained from the METOP/ASCAT-A or ASCAT-B satellite scatterometers.

The matchup criteria between the ReSI specular points and ASCAT-A/B were set to allow a maximum separation of 1° of latitude/longitude and 1 h. ASCAT wind speed data were taken from Level 1B Swath products with a resolution of 25 km, available from the Physical Oceanography Distributed Active Archive Center (https://podaac.jpl.nasa.gov/). Standard ASCAT data quality flags were applied, including rain flags, in order to avoid any potentially rain-contaminated ASCAT wind data in the subsequent assessment of TDS-1 GNSS-R winds. Fortuitously, the TDS-1 orbit at the start of the mission was particularly favorable to collocation with ASCAT-A/B, with almost 70% of all ReSI data over the ocean finding a suitable matchup with at least one of ASCAT-A or ASCAT-B within 1° and 1 h.

Figure 2 shows two examples of 1 Hz DDMs processed on board, obtained on two separate occasions with wind speed of 3 m/s (according to collocated ASCAT data) but different values of antenna gain at the specular point (AGSP). The dimensions (resolution) of the DDMs are 128 bins in delay (0.25 chip spacing) and 20 bins in Doppler frequency (500 Hz spacing). The DDMs show the expected "horseshoe"-shaped characteristic of spaceborne GNSS-R correlated power over the ocean, with the DDM peak corresponding to the area around the specular point on the ocean surface. Since TDS-1 was operating in uAGC mode, absolute power levels are unknown. One observes, nevertheless, the very significant effect on peak power levels of the AGSP, as well as the asymmetry in the DDM associated with the modulation of the correlated power by the antenna pattern.

The highest wind speed encountered so far was observed in the Atlantic Sector of the Southern Ocean on 31 October 2014 when collocated ASCAT data reported winds up to 27.9 m/s. The 1 Hz DDM corresponding to these high wind conditions is shown in Figure 3. Even without calibration, it is easy to see that the DDM is much broader and power levels are much lower at high winds due to increased scatter away from the forward-scattering direction toward the receiver. Nevertheless, Figure 3 convincingly demonstrates that
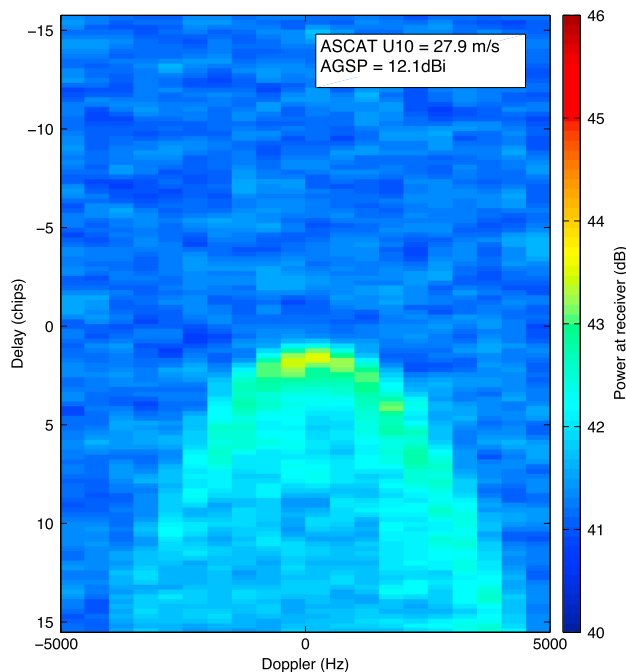
Figure 2. Two examples of TDS-1 ReSI onboard-processed 1 Hz delay-Doppler maps obtained for a wind speed of 3 m/s (according to collocated ASCAT data) for two values of Antenna Gain at the Specular Point (AGSP), namely, (a) 13.3 dBi (at the peak of the main lobe) and (b) 7.2 dBi (at −6 dB from the peak gain).

TDS-1 ReSI was able to detect GPS-reflected signals and maintain good data quality and integrity even in those high wind conditions.

4. Wind Speed Inversion and the Bistatic Radar Equation

Many methods and algorithms have been proposed in the literature to retrieve ocean surface roughness, wind speed, or sea state from GNSS-R measurements (see, for example, *Zavorotny et al.* [2014], *Clarizia et al.* [2014], *Marchan-Hernandez et al.* [2010] among others, and the references therein). In this paper, a wind inversion algorithm is proposed based on the DDM correlated power around the specular point and the GNSS-R Bistatic Radar Equation (BRE).

Figure 3. TDS-1 ReSI onboard-processed 1 Hz delay-Doppler map obtained for a wind speed of 27.9 m/s (according to collocated ASCAT data) in the Atlantic sector of the Southern Ocean on 31 October 2014.

The BRE encapsulates the dependence of the GNSS-R DDM on rough ocean properties [*Zavorotny and Voronovich*, 2000; *Gleason*, 2006] as follows:

$$\langle |Y(\tau,f)|^2 \rangle = \frac{P_t G_t \lambda^2 T_i^2}{(4\pi)^3} \iint_A \frac{G_r \Lambda^2(\tau) S^2(f)}{R_t^2 R_r^2} \sigma^0 \mathrm{d}A \tag{1}$$

where $\langle |Y(\tau,f)|^2 \rangle$ is the ensemble mean of the correlation power as a function of the time delay (τ) and the frequency offset (f), P_t and G_t are the GPS transmitter power and antenna gain, λ is the carrier wavelength (L-band), T_i is the coherent integration time, G_r is the receiver antenna pattern, R_t and R_r are respectively the transmitter-to-surface and surface-to-receiver ranges, Λ^2 and S^2 are the components of the Woodward Ambiguity Function (WAF) in delay (triangular function) and Doppler frequency (sinc function), respectively, dA is the surface element of the scattering area A, and σ^0 is the normalized bistatic radar cross section. With some simplifying assumptions, equation (1) can be rewritten so that

$$\langle \sigma^0 \rangle = KP_r \left[\iint_A \frac{G_r \Lambda^2(\tau) S^2(f)}{R_t^2 R_r^2} \mathrm{d}A \right]^{-1} \tag{2}$$

where $\langle \sigma^0 \rangle$ represents the average σ^0 associated with the received power, P_r, for surface area A, and K is a constant equal to $\frac{P_t G_t \lambda^2 T_i^2}{(4\pi)^3}$. The simplifying assumptions leading to equation (2) are as follows: (a) The σ^0 is constant over the area A and can be taken out of the integral in equation (1). (b) Differences in P_t and G_t for different GPS PRN are second-order effects, so that P_t and G_t can be assumed constant to a first approximation.

Clearly, the second assumption neglects the known differences in the direct signal strength of different GPS transmitters, but at present the direct signal levels are not available from the TDS-1 data sets. In addition, there will be intermittent fluctuations in the signal strength of the reflected signals due to atmospheric effects (e.g., scintillation). These secondary terms are also overlooked at this stage but will need to be addressed in the future.
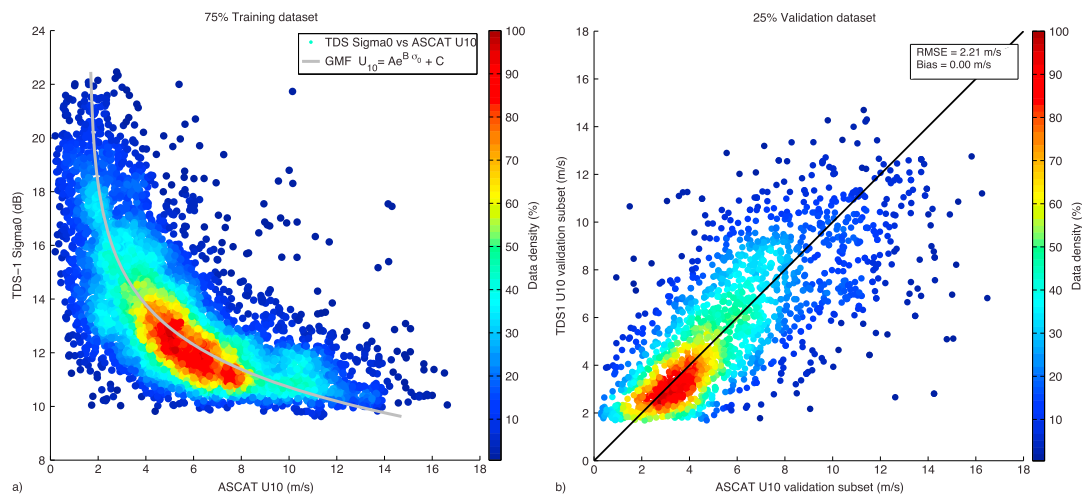
The content of the square brackets in equation (2) is determined entirely by the geometry of the bistatic scattering at the specular point and has to be computed numerically. The numerical computation accounts for the velocities and positions of the transmitter and receiver, the attitude of the receiver platform, and the projected receiver antenna pattern on the surface. Clearly, uncertainties in platform attitude will directly impact the antenna gain at the specular point and, therefore, σ^0.

In contrast, the term P_r is estimated from the measured DDM. Here P_r is computed from the signal-to-noise ratio (SNR) of the correlated power around the specular point. SNR is calculated as the ratio of the average signal power (S) in a box located around the peak of the DDM, and the average noise power (N) measured in a noise box in the signal-free area of the DDM. Minor variants of the definition of the SNR make little difference to the final results. The sizes of the signal and noise boxes are fixed. The noise box spans all Doppler bins and four delay bins starting from the first delay available in the DDM. The size of the signal box determines the surface area (A) that contributes to the measured power and, therefore, the spatial resolution of the measurement. Here the dimensions of the signal box are chosen to achieve a spatial resolution close to that of ASCAT, namely, 25 km. The dimensions of the signal box were one chip (four delay bins) by 1500 Hz (3 Doppler bins) corresponding to a spatial resolution between 22 and 30 km (median value 25 km) depending on the elevation angle of the specular point. Since the position of the peak fluctuates in both delay and Doppler space (for example, due to changes in the range to the Earth surface), the signal box is positioned dynamically around the peak using an automatic peak detection scheme. The automatic peak detection is based on the application of a median filter and extraction of the local maxima in the DDM.

5. Geophysical Model Function and Early Validation Against ASCAT Winds

In reality, the ReSI SNR cannot be equated directly with P_r since the measured SNR is also affected by other effects including changes in system noise levels, speckle noise, the receiver instrument gain setting (which is unknown when ReSI operates in uAGC mode), and fluctuations in signal strength due to atmospheric effects (for example, amplitude scintillation caused by irregularities in electron density in the ionosphere; see, e.g., *Dubey et al.* [2005]). The original purpose of the AGC is to automatically adjust the GNSS receiver gain to make optimal use of the available dynamic range and enable the detection of even low power signals. While this

Figure 4. (a) TDS-1 ReSI uAGC mode σ^0 versus collocated ASCAT wind speed for SNR $\geq$ 3 dB for the Training data set, showing (in grey) the preliminary GMF of the form $U_{10} = Ae^{B\sigma^0} + C$ with values of A, B, and C equal to 676.0, 0.4097, and 1.622, respectively; (b) TDS-1 ReSI wind speed retrieved with the BRE algorithm versus collocated ASCAT winds for the Validation data set. This example validation data set yields bias and RMSE values of 0.004 m/s and 2.213 m/s, respectively, and is statistically representative of the overall BRE retrieval performance.

feature is desirable to ensure signal detection, it introduces an unknown factor in the DDM power levels which could obscure the relationship between SNR and ocean roughness. One way of minimizing these unknown effects is to limit analyses, in the first instance, to high SNR signals when the impact is likely to be less pronounced. This is the approach adopted here whereby the ReSI/ASCAT matchup data set is reduced to include only ReSI reflections for which the SNR $\geq$ 3 dB (an arbitrary threshold corresponding to signals for which the peak power is more than twice the noise level).

The effect of the 3 dB SNR threshold is to remove some high wind samples and to reject specular points obtained outside the main lobe. Focusing on data in the main lobe of the antenna, where AGSP gradients are smallest, also has the advantage of reducing the sensitivity to possible attitude errors. The remaining matchup data set is much reduced, to about 20% of the original collocated data set, but nevertheless counts 7514 data points retained for analysis. The retained data set is further divided into a randomly selected Training set (75% of samples) used for the development of the Geophysical Model Function (GMF) and a Validation set (25% of samples) reserved for retrieval performance assessment.

Figure 4a shows the relationship observed with the Training set between the (uAGC mode) ReSI σ^0 and the collocated ASCAT wind speed. Colors indicate data density relative to the distribution peak. The data cloud clearly shows GNSS-R σ^0 decreasing rapidly with increasing wind speed, in a manner that is reminiscent of the behavior of nadir altimeter σ^0 against wind speed [see, for example, *Gommenginger et al.*, 2002; *Abdalla*, 2012, and references therein]. Here we find that the behavior is well captured in the first instance by a simple function of the form $U_{10} = Ae^{B\sigma^0} + C$, shown as a grey line in Figure 4a. Using ordinary least squares fit, the values of A, B, and C are 676.0, 0.4097, and 1.622, respectively. Figure 4b presents the TDS-1 ReSI retrieved wind speed obtained by applying the GMF in Figure 4a to the Validation set. The retrieved wind speed is unbiased (bias = 0 m/s) and reports a root-mean-square error of 2.2 m/s.

6. Summary and Conclusions

First results were presented of ocean surface wind speed retrieval from reflected GPS signals collected by the UK TechDemoSat-1 satellite launched in July 2014. The extensive data set of new spaceborne GNSS-R observations collected since 1 September 2014 was described, with examples of onboard-processed delay-Doppler maps that demonstrate excellent data quality from low Earth orbit for wind speed up to 27.9 m/s. A wind speed retrieval algorithm based on the GNSS-R Bistatic Radar Equation and the signal-to-noise ratio was developed and validated against collocated ASCAT wind speed. Analyses were restricted to GPS reflections with SNR greater than 3 dB to mitigate the unknown impact of other factors affecting power levels on the relation between the measured GNSS-R signals and ocean wind speed. The ReSI uAGC mode σ^0 showed a rapidly decreasing behavior against wind speed, similar to the relation seen for satellite nadir altimeters.

Even without calibration and potentially large satellite attitude errors, the preliminary Geophysical Model Function presented in this paper leads to retrieved TDS-1 wind speeds that are unbiased \emph{with} root-mean-square errors of 2.2 m/s for winds between 3 and 18 m/s.

This study represents the first comprehensive in-orbit demonstration of the GNSS-R technique and confirms the capability of low-cost, low-mass, and low-power GNSS-R receivers such as ReSI to contribute significantly to global ocean surface wind monitoring from low Earth orbit altitudes. The findings give new strength to the prospect of affordable satellite constellations to deliver necessary improvements in spatiotemporal sampling of weather systems in combination with existing satellite wind data. However, full demonstration of the wide-swath capabilities of spaceborne GNSS-R was not possible due to insufficient knowledge about the TDS-1 satellite attitude and other factors linked to instrument behavior and power level fluctuations. Future work will focus on reducing uncertainties linked to satellite attitude and antenna gain at the specular point that should yield further improvements in wind speed retrieval performance. More work is needed also to understand and manage the origins of observed power fluctuations, thereby enabling the assessment and exploitation of low SNR signals and make it possible to establish the wide-swath capability of the technique.

References

Abdalla, S. (2012), Ku-band radar altimeter surface wind speed algorithm, *Mar. Geod.*, *35*(Sup. 1), 276–298.

Auber, J.-C., A. Bibaut, and J.-M. Rigal (1994), Characterization of multipath on land and sea at GPS frequencies, in *Proceedings of the 7th International Technical Meeting of the Satellite Division of The Institute of Navigation (ION GPS 1994)*, pp. 1155–1171, Salt Palace Convention Center, Salt Lake City, Utah.

Cardellach, E., F. Fabra, O. Nogués-Correig, S. Oliveras, S. Ribó, and A. Rius (2011), GNSS-R ground-based and airborne campaigns for ocean, land, ice, and snow techniques: Application to the GOLD-RTR data sets, *Radio Sci.*, *46*(6), RS0C04, doi:10.1029/2011RS004683.

Carreno-Luengo, H., H. Park, A. Camps, F. Fabra, and A. Rius (2013), GNSS-R derived centimetric sea topography: An airborne experiment demonstration, *IEEE J. Sel. Top. Appl. Earth Observations Remote Sens.*, *6*(3), 1468–1478.

Clarizia, M., C. Gommenginger, S. Gleason, M. Srokosz, C. Galdi, and M. Di Bisceglie (2009), Analysis of GNSS-R delay-Doppler maps from the UK-DMC satellite over the ocean, *Geophys. Res. Lett.*, *36*, L02608, doi:10.1029/2008GL036292.

Clarizia, M. P., C. S. Ruf, P. Jales, and C. Gommenginger (2014), Spaceborne GNSS-R minimum variance wind speed estimator, *IEEE Trans. Geosci. Remote Sens.*, *52*(11), 6829–6843, doi:10.1109/TGRS.2014.2303831.

Dubey, S., R. Wahi, E. Mingkhwan, and A. Gwal (2005), Study of amplitude and phase scintillation at GPS frequency, *Indian J. Radio Space Phys.*, *34*(6), 402–407.

Garrison, J. L., S. J. Katzberg, and M. I. Hill (1998), Effect of sea roughness on bistatically scattered range coded signals from the Global Positioning System, *Geophys. Res. Lett.*, *25*(13), 2257–2260.

Gleason, S. (2006), Remote sensing of ocean, ice and land surfaces using bistatically scattered GNSS signals from low Earth orbit, Univ. of Surrey, U. K.

Gleason, S., and D. Gebre-Egziabher (2009), *GNSS Applications and Methods*, Artech House, Boston, Mass.

Gommenginger, C. P., M. A. Srokosz, P. G. Challenor, and P. D. Cotton (2002), Development and validation of altimeter wind speed algorithms using an extended collocated buoy/topex dataset, *IEEE Trans. Geosci. Remote Sens.*, *40*(2), 251–260.

Hall, C., and R. Cordey (1988), Multistatic scatterometry, in *Geoscience and Remote Sensing Symposium, 1988. IGARSS'88. Remote Sensing: Moving Toward the 21st Century., International*, vol. 1, pp. 561–562, IEEE, U. K.

Jales, P., and M. Unwin (2015), Mission description - GNSS reflectometry on TDS-1 with the SGR-ReSI, Tech. Rep. SSTL rep. 0248367 Revision 001, Surrey Satellite Technology Ltd, Guildford, U. K. [Available at http://www.merrbys.co.uk.]

Katzberg, S. J., O. Torres, and G. Ganoe (2006), Calibration of reflected GPS for tropical storm wind speed retrievals, *Geophysical Research Letters*, *33*, L18602, doi:10.1029/2006GL026825.

Komjathy, A., M. Armatys, D. Masters, P. Axelrad, V. Zavorotny, and S. Katzberg (2004), Retrieval of ocean surface wind speed and wind direction using reflected GPS signals, *J. Atmos. Oceanic Technol.*, *21*(3), 515–526.

Lowe, S. T., C. Zuffada, Y. Chao, P. Kroger, L. E. Young, and J. L. LaBrecque (2002), 5-cm-precision aircraft ocean altimetry using GPS reflections, *Geophysical Research Letters*, *29*(10), 1375, doi:10.1029/2002GL014759.

Marchan-Hernandez, J., E. Valencia, N. Rodriguez-Alvarez, I. Ramos-Perez, X. Bosch-Lluis, A. Camps, F. Eugenio, and J. Marcello (2010), Sea-state determination using GNSS-R data, *IEEE Geosci. Remote Sens. Lett.*, *7*(4), 621–625.

Martin-Neira, M. (1993), A Passive Reflectometry and Interferometry System (PARIS): Application to ocean altimetry, *Ecol. Soc. Am. J.*, *17*, 331–355.

Nogues-Correig, O., S. Ribo, J. C. Arco, E. Cardellach, A. Rius, E. Valencia, J. M. Tarongí, A. Camps, H. van der Marel, and M. Martín-Neira (2010), The proof of concept for 3-cm altimetry using the Paris interferometric technique, in *International Geoscience and Remote Sensing Symposium (IGARSS)*, pp. 3620–3623, IEEE, Honolulu, Hawaii.

Rius, A., J. M. Aparicio, E. Cardellach, M. Martín-Neira, and B. Chapron (2002), Sea surface state measured using GPS reflected signals, *Geophys. Res. Lett.*, *29*(23), 21–22, doi:10.1029/2002GL015524.

Ruf, C. S., S. Gleason, Z. Jelenak, S. Katzberg, A. Ridley, R. Rose, J. Scherrer, and V. Zavorotny (2012), The CYGNSS nanosatellite constellation hurricane mission, in *International Geoscience and Remote Sensing Symposium (IGARSS)*, pp. 214–216, IEEE, Munich, Germany.

Ruffini, N. G., F. Soulat, M. Caparrini, O. Germain, and M. Martín-Neira (2004), The eddy experiment: Accurate GNSS-R ocean altimetry from low altitude aircraft, *Geophys. Res. Lett.*, *31*, L12306, doi:10.1029/2004GL019994.

Valencia, E., A. Camps, N. Rodriguez-Alvarez, I. Ramos-Perez, X. Bosch-Lluis, and H. Park (2011), Improving the accuracy of sea surface salinity retrieval using GNSS-R data to correct the sea state effect, *Radio Sci.*, *46*, RS0C02, doi:10.1029/2011RS004688.

Zavorotny, V., S. Gleason, E. Cardellach, and A. Camps (2014), Tutorial on remote sensing using GNSS bistatic radar of opportunity, *IEEE Geosci. Remote Sens. Mag.*, *2*(4), 8–45.

Zavorotny, V. U., and A. G. Voronovich (2000), Scattering of GPS signals from the ocean with wind remote sensing application, *IEEE Trans. Geosci. Remote Sens.*, *38*(2), 951–964.